Acta Pharmaceutica Sinica B 2025;15(2):1112−1125

Chinese Pharmaceutical Association
Institute of Materia Medica, Chinese Academy of Medical Sciences

Acta Pharmaceutica Sinica B

www.elsevier.com/locate/apsb
www.sciencedirect.com

ORIGINAL ARTICLE

NO-releasing double-crosslinked responsive hydrogels accelerate the treatment and repair of ischemic stroke

Wen Guo[a,†], Cheng Hu[b,†], Yue Wang[b], Wen Zhang[b], Shaomin Zhang[a], Jin Peng[a], Yunbing Wang[b,*], Jinhui Wu[a,*]

[a]*Center of Gerontology and Geriatrics, National Clinical Research Center for Geriatrics, West China Hospital, Sichuan University, Chengdu 610041, China*
[b]*National Engineering Research Center for Biomaterials, College of Biomedical Engineering, Med-X Center for Materials, Sichuan University, Chengdu 610064, China*

Received 8 September 2024; received in revised form 28 November 2024; accepted 7 December 2024

KEY WORDS

Hydrogel;
Nitric oxide;
Ischemic stroke;
Angiogenesis;
Anti-inflammation;
Macrophage migration inhibitory factor;
Neuroprotective;
Double-crosslinked

Abstract Stroke is a global disease that seriously threatens human life. The pathological mechanisms of ischemic stroke include neuroinflammation, oxidative stress, and the destruction of blood vessels at the lesion site. Here, a biocompatible *in situ* hydrogel platform was designed to target multiple pathogenic mechanisms post-stroke, including anti-inflammation, anti-oxidant, and promotion of angiogenesis. Double-crosslinked responsive multifunctional hydrogels could quickly respond to the pathological microenvironment of the ischemic damage site and mediate the delivery of nitric oxide (NO) and ISO-1 (inhibitor of macrophage migration inhibitory factor, MIF). The hydrogel demonstrated good biocompatibility and could scavenge reactive oxygen species (ROS) and inflammatory cytokines, such as interleukin-6 (IL-6), interleukin-10 (IL-10), and MIF. In a mouse stroke model, hydrogels, when situated within the microenvironment of cerebral infarction characterized by weak acidity and elevated ROS release, would release anti-inflammatory nanoparticles rapidly that exert an anti-inflammatory effect. Concurrently, NO was sustained release to facilitate angiogenesis and provide neuroprotective effects. Neurological function was significantly improved in treated mice as assessed by the modified neurological severity score, rotarod test, and open field test. These findings indicate that the designed hydrogel held promise for sustained delivery of NO and ISO-1 to alleviate cerebral ischemic injury by responding to the brain's pathological microenvironment.

*Corresponding authors.
E-mail addresses: yunbing.wang@scu.edu.cn (Yunbing Wang), wujinhui@scu.edu.cn (Jinhui Wu).
[†]These authors made equal contributions to this work.
Peer review under the responsibility of Chinese Pharmaceutical Association and Institute of Materia Medica, Chinese Academy of Medical Sciences.

https://doi.org/10.1016/j.apsb.2025.01.005

1. Introduction

Stroke is a global disease that poses a serious threat to human life and health, and it is one of the leading causes of death worldwide[1]. Ischemic stroke, also known as cerebral infarction, is the most common type of stroke, accounting for approximately 80% of cases[2]. In conventional treatment plans, due to the narrow therapeutic window, the majority of patients with cerebral infarction failed to benefit and may also suffer from associated complications[3]. Moreover, the process of ischemic injury and chronic recovery is highly complex, with treatment mechanisms characterized by multiple targets and pathways. The efficacy of current neuroprotective agents is also relatively limited[4]. During cerebral ischemia, cerebral blood perfusion is insufficient, leading to excessive production of reactive oxygen species (ROS) in the affected regions, which in turn triggers a cascade of inflammatory responses and apoptosis[5,6]. Even after blood supply is restored, the process of ischemia-reperfusion can still induce ROS-mediated inflammatory reactions, resulting in irreversible brain damage[7-9]. Therefore, the design of hydrogels that can respond to the pathological microenvironment and ameliorate it is of significant research interest[10]. Intravenous drug administration is also widely used in the treatment of cerebral infarction. However, due to the severe impairment of the blood−brain barrier in the early stages of stroke, the efficiency of intravenous drug delivery is not as effective as *in situ* drug administration[11-14]. Consequently, we have specifically chosen *in situ* injection of hydrogels for the treatment of cerebral infarction[15].

Following the occurrence of cerebral infarction, the brain undergoes metabolic disorders in cells due to ischemia and hypoxia, leading to a series of pathophysiological processes[16-18]. Excitotoxicity, oxidative stress, and mitochondrial dysfunction can induce various cellular cascade reactions, ultimately leading to neuronal apoptosis, necrosis, and autophagy[19,20]. Concurrently, the aggregation of neutrophils in the ischemic core area exacerbates oxidative stress and blood−brain barrier damage[21]. Thus, controlling inflammation in the ischemic microenvironment before neurorepair is necessary[22]. In addition to managing the inflammatory response after cerebral infarction, promoting angiogenesis and re-establishing blood flow are also crucial pathophysiological mechanisms[23].

Macrophage migration inhibitory factor (MIF) is an inflammatory and stress-regulatory cytokine with chemokine-like functions. It directly or indirectly promotes the expression of a multitude of pro-inflammatory factors, such as interleukin-1β (IL-1β), tumor necrosis factor-α (TNF-α), and interleukin-6 (IL-6)[24-26]. Its specific inhibitor (ISO-1) exhibits good inhibitory effects on MIF and can suppress the expression of downstream molecules critical for blood−brain barrier disruption, matrix metalloproteinase-9 (MMP-9), as well as other inflammatory factors in brain tissue, thereby reducing the infarct area, alleviating blood−brain barrier damage, and improving neurological function deficits[27,28]. Nitric oxide (NO), as a signaling molecule, has a broad range of functions within the body[29]. NO is one of the end products in the angiogenesis signaling cascade, synergizing with growth factors to promote angiogenesis in capillaries, and playing an important role in collateral circulation and neovascularization after ischemic injury[30,31]. In addition to its effects on blood vessels, NO also has anti-neuroinflammatory and neuroprotective effects[32,33].

Based on previous research, we have constructed an *in situ* hydrogel platform for anti-inflammation, angiogenesis promotion, and neuroprotection, which is expected to become a new therapeutic method for the recovery of ischemic injury after stroke. Initially, we synthesized a NO donor and prepared the gelatin−NO (Gel−NO) polymer through an amination reaction between the carboxyl group of the NO donor and the amine groups of gelatin. Subsequently, the Gel−NO polymer and oxidized dextran (ODex) were successfully crosslinked *via* a Schiff base reaction to fabricate an acid-responsive hydrogel capable of releasing NO. To confer anti-inflammatory properties to the hydrogel, we aimed to incorporate a MIF inhibitor into the hydrogel system. Considering its hydrophobicity, we selected Pluronic F-127 (PF127) polymers modified with phenylboronic acid at both ends as the delivery vehicle. On one hand, PF127BA can effectively encapsulate ISO-1, and on the other hand, the phenylboronic acid groups on the surface of PF127B@ISO-1 nanoparticles can form boronate esters with the vicinal diols of ODex, constituting a secondary crosslinking mechanism within the hydrogel. The advantage of this approach is that it not only tightly anchors the nanoparticles within the hydrogel matrix but also allows for intelligent response and release upon exposure to acidity and ROS. Furthermore, it can effectively scavenge ROS through the cleavage of boronate esters (Scheme 1).

In summary, double-crosslinked responsive multifunctional hydrogel loaded with PF127B@ISO-1 nanoparticles could prevent neuronal apoptosis, reduce inflammation, and eliminate free radicals to alleviate ischemic injury in mouse hippocampal neuronal cell line (HT22) after oxygen-glucose deprivation (OGD) model. In the photothrombotic induction model, the hydrogel was injected *in situ* in the cerebral infarction area to exert neuroprotection, anti-inflammation, and angiogenesis-promoting functions, ultimately achieving neurological function recovery after ischemic stroke. Both *in vitro* and *in vivo* experimental results confirmed that the *in situ* hydrogel platform for sustained release of NO and the small molecule inhibitor ISO-1 could alleviate cerebral ischemic injury through multiple pathways, providing a more promising direction for the treatment of ischemic stroke.

2. Materials and methods

2.1. Chemicals and reagents

Gelatin, dextran, bromoacetic acid, silver nitrate, anhydrous acetonitrile, dichloromethane, *N*-hydroxysuccinimide (NHS), 1-ethyl-3-(3-dimethylaminopropyl) carbodiimide (EDC), 2-(*N*-morpholino) ethanesulfonic acid (MES), sodium periodate, Pluronic F127 (PF127), 4-carboxyphenylboronic acid, 4-(dimethylamino)pyridine (DMAP), and tetrahydrofuran were purchased from Adamas (Shanghai, China). ISO-1 was obtained

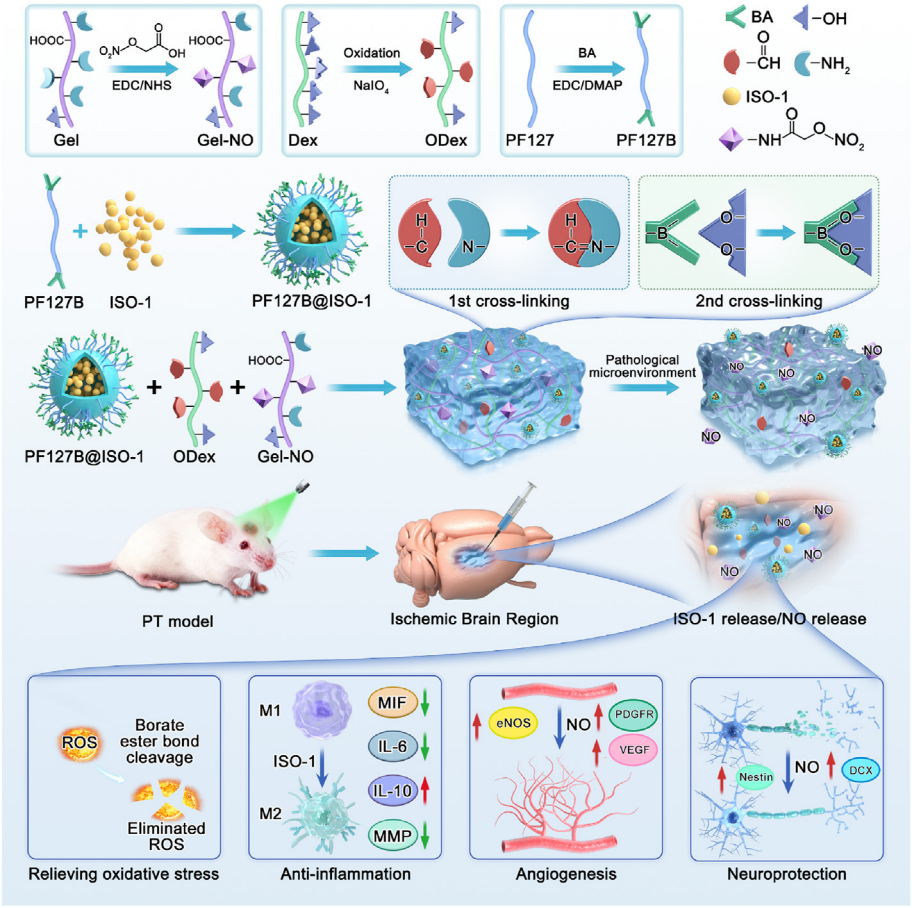

Scheme 1 The preparation process and drug release mechanism of the double-crosslinked hydrogel.

from MedChemExpress (Shanghai, China). Cell Counting Kit-8(CCK-8 assay kit), ROS assay kit, and NO assay kit were purchased from Beyotime Biotech Inc. (Shanghai, China). Dulbecco's modified Eagle's medium (DMEM) media, fetal bovine serum (FBS), and penicillin-streptomycin double antibiotics were purchased from Gibco (New York, NY, USA).

2.2. *Synthesis of Gel−NO and ODex*

Synthesis of Gel−NO: Bromoacetic acid (2.00 g, 14.3 mmol) and silver nitrate (3.70 g, 21.8 mmol) were stirred in anhydrous acetonitrile (80 mL) at 70 °C for 18 h. After filtration, the product was concentrated under vacuum, and dichloromethane (100 mL) was added. The mixture was incubated at room temperature for 2 h, filtered again, and the dichloromethane was removed to obtain the yellow oily nitroxy acetic acid. 2-(Nitroxy) acetic acid (3.5 mL), NHS (6.3 g), and EDC (10.5 g) were dissolved in 100 mL of MES buffer solution (pH 6.0) to activate the carboxyl group. After 2 h, gelatin (5.5 g) was added and stirred for 48 h, and then dialyzed with deionized water (DW) and lyophilized. Synthesis of ODex: 10.0 g of dextran and 8.0 g of sodium periodate were dissolved in DW and stirred at 37 °C for 4 h. Then, 1.2 mL of ethylene glycol was added to the above solution and stirred for 2 h to mix evenly. Finally, it was dialyzed with DW for 48 h and lyophilized to obtain ODex. Proton nuclear magnetic resonance (^{1}H NMR) confirmed the synthesis of these substances.

2.3. *Preparation and characterization of PF127B and PF127B@ISO-1 nanoparticles*

20 g of PF127 was dissolved in dichloromethane, followed by the addition of 1.5 g of 4-carboxyphenylboronic acid, 1.92 g of EDC, and 611 mg of DMAP, and reacted under nitrogen protection to form PF127B. Synthesis of PF127B nanoparticles: 100 mg of PF127B was dissolved in 5 mL of tetrahydrofuran and processed with a rotary evaporator at 40 °C for 15 min and dried in an oven at 40 °C for 20 min to obtain PF127BA nanoparticles. PF127B@ISO-1 nanoparticles: 100 mg of PF127B and 10 mg of ISO-1 were each dissolved in 5 mL of tetrahydrofuran, with subsequent steps being the same as the synthesis of PF127B nanoparticles. The particle size of PF127BA and PF127B@ISO-1 was measured by dynamic light scattering (DLS, Malvern Instruments Ltd., Zetasizer, Malvern, UK). Particles were observed using a transmission electron microscope (TEM, Hitachi, Ltd., H600, Tokyo, Japan).

2.4. *Preparation of hydrogels*

The lyophilized polymer was dissolved in phosphate buffered saline (PBS), and the Gel−NO and ODex solutions were mixed in equal proportions to form a hydrogel rapidly. 1 mL of hydrogel containing PF127BA (0.2 mg) or PF127B@ISO-1 (0.2 mg) was abbreviated as G_{NO}−OD HG@ NPs or G_{NO}−OD HG@ISO-1

NPs. The three groups of hydrogels were named as follows: G_{NO}−OD HG, Hydrogel grafted with NO; G_{NO}−OD HG@ NPs, Hydrogel with empty nanoparticles; G_{NO}−OD HG@ISO-1 NPs, hydrogel encapsulating ISO-1 loaded nanoparticles.

2.5. Characterization of hydrogels

The rheological behavior was measured using a rheometer (Anton Paar GmbH, MCR302, Graz, Austria). Frequency sweeps were performed with oscillation frequencies ranging from 0.1 to 10 rad/s and a fixed strain of 1%. Strain sweeps ranged from 0.01% to 1000% with a fixed oscillation frequency of 1 rad/s. The fracture structure of the lyophilized hydrogel was observed using scanning electron microscopy (SEM, Hitachi, Ltd., S4800, Tokyo, Japan).

In vitro drug release was detected using UV−Vis and the Griess assay kit (NO assay kit, Beyotime Biotech Inc., China). G_{NO}−OD HG@ISO-1 NPs were placed in dialysis bags containing 10 mL of PBS (pH = 7.4) and 10 mL of PBS (pH = 6.5) + 1 mmol/L H_2O_2 solution ($n = 3$). On Days 0, 0.25, 0.5, 1, 2, 3, 4, 7, and 14, 2 mL of dialysate was taken and the release of ISO-1 was measured by UV spectrophotometry, and the release of NO was measured using the Griess assay kit.

2.6. OGD model

HT22 and BV2 were purchased from Procell Life Science & Technology Co., Ltd. (Wuhan, China). Cells were routinely cultured with complete medium (DMEM high glucose, 10% FBS, 1% penicillin/streptomycin). The complete medium was replaced with D-glucose-free DMEM and placed in a container with 37 °C, 5% CO_2, 94% N_2, and 1% O_2 for 2 h, then replaced with complete medium and placed in a regular environment to establish the OGD model. Control group cells were cultured routinely.

2.7. Cell compatibility and metabolic activity assay

CCK-8 and Live/Dead staining evaluated cell compatibility and metabolic activity. First, 1 mL of hydrogel was immersed in DMEM complete medium (10 mL) for 48 h to obtain the dialysis solution; next, HT22 and BV2 cells were seeded in a 96-well plate (3×10^3 cells/well) and subjected to OGD, then replaced with hydrogel dialysis solution and treated for 48 h. Cell viability was measured using the CCK-8 assay kit. FDA/PI staining kit (BestBio, Nanjing, China) was used, and cell survival was observed under a fluorescence microscope (Leica, DMI 4000, Wiesbaden, Germany).

2.8. ELISA assay

BV2 cells were seeded in a 6-well plate. After 48 h of OGD and hydrogel treatment, the cell supernatant was collected, and the protein concentrations of IL-6, IL-10, and MIF were quantitatively determined using an ELISA assay kit (Boster, Wuhan, China) according to the instructions.

2.9. Photothrombotic (PT) stroke model

The photothrombotic cerebral ischemia model was used to induce focal cortical ischemia. All experimental procedures were executed according to the protocols approved by the Animal Ethics Committee of Sichuan University (No.20240226245). Male Sprague Dawley (SD) mice were used for the animal experiments (Ensiweier Experimental Animals Co., Ltd., Beijing, China). First, mice were anesthetized with isoflurane, and 1% Bengal Rose (10 μL/g body weight, Aladdin, Shanghai, China) was injected intraperitoneally; 15 min later, the mice were fixed in a stereotactic apparatus (RWD Life Science, Shenzhen, China), and a 3 mm bone window was made 2 mm lateral to the anterior fontanelle with a trephine. Then, the motor cortex area was irradiated for 8 min through the bone window using a 100-mW cold light illuminator, and the incision was sutured after irradiation. During the recovery period, the health status of the mice was monitored daily.

2.10. Experimental grouping

After 3 days of completing the cerebral ischemia model, the mice were anesthetized with isoflurane and fixed on a stereotactic apparatus. Hydrogel was injected into the central area of the infarction zone 2 mm below the endocranium using a micro syringe, with 2 μL injected into the infarction area of each mouse. After the injection, the needle was slowly withdrawn after staying for 5 min, and the incision was disinfected with iodine and sutured. Experimental animals were randomly divided into the following 5 groups: (a) Sham operation group (sham), (b) Photothrombotic ischemic stroke model (PT), (c) Ischemic stroke model injected with Gel−NO hydrogel group (G_{NO}−OD HG), (d) Ischemic stroke model injected with Gel−NO+empty PF127BA nanoparticle hydrogel group (G_{NO}−OD HG@ NPs), (e) Ischemic stroke model injected with Gel−NO+PF127B@MIF inhibitor (ISO-1) nanoparticle hydrogel group (G_{NO}−OD HG@ISO-1 NPs).

2.11. Neurological function assessment

Neurological function was measured using the modified neurological severity score (mNSS), rotarod test, and open field test after stroke in mice. Mice were trained for 3 consecutive days before stroke modeling for mNSS, rotarod test, and open field test. Neurobehavioral tests were performed on Days 0, 1, 7, 14, and 21 after modeling. The mNSS ranges from 0 to 18 points, reflecting changes in motor, sensory, balance, and reflex functions. Higher scores indicate more severe neurological deficits, while lower scores indicate neurological function recovery. The rotarod test was performed on a fixed-speed rotarod device to assess the mouse's motor coordination and balance ability; the stay time was recorded by the sensor. The longer time mice stay, the better the coordination and balance ability they have. Open field test: The experimental animals were placed in a 25 cm × 25 cm × 25 cm empty box, with a single mouse placed in the center of the open field and allowed to move freely for 5 min. The activity distance and time in the central and peripheral areas were analyzed to evaluate the spontaneous activity of the experimental animals.

2.12. Laser speckle blood flow imaging

On Days 1 and 21 after mouse modeling, the mice were continuously anesthetized with an animal isoflurane gas anesthesia device. The anesthetized mice were placed on the imaging stage of the laser speckle blood flow instrument (RWD Life Science, RFLSI ZW, Shenzhen, China), the entire brain of the mouse was exposed, the position was adjusted, and the automatic focusing mirror was used to make the image clear and complete. The parameters of the laser speckle blood flow instrument were

adjusted, the laser viewing light source was 780 nm; the irradiation area was through a charge-coupled device (CCD), the exposure time was 5 ms, the frame frequency was 30 fps, the imaging speed was 200 frames per second, and a 1280 × 960-pixel image was obtained. The region of interest (ROI) was outlined to observe vascular changes and read blood perfusion values.

2.13. *RNA sequencing and analysis*

Brain tissue was taken for RNA-seq testing 21 days after hydrogel injection. Total RNA was isolated using the RNeasy mini kit (Qiagen, Dusseldorf, Germany). The cBot and the library generated the gene cluster and then sequenced it on the Illumina NovaSeq 6000 (Santiago, CA, USA). Library construction and sequencing were completed by Metware Biotechnology Co., Ltd. (Wuhan, China).

2.14. *Statistical analysis*

Values are expressed as mean ± standard deviation (SD). ANOVA statistical methods were used to compare differences between groups. Data analysis was performed using GraphPad Prism software (Santiago, CA, USA). $*P < 0.05$, $**P < 0.01$, $***P < 0.001$, and $****P < 0.0001$.

3. Results and discussion

3.1. *Preparation and characterization of materials*

ODex and NO grafted gelatin (Gel−NO) were crosslinked through the Schiff base reaction to form a hydrogel (G_{NO}−OD HG). To ascertain the optimal ratio for the synthesis of hydrogels, we took both injectability and drug release into account, ultimately selecting a ratio of oxidized dextran to gelatin of 1:1 for our experiment (Supporting Information Fig. S1). In simple terms, dextran was oxidized with sodium periodate to form ODex. Gel−NO was synthesized by the reaction of 2−(nitroxy) acetic acid with gelatin under a catalytic system of EDC/NHS and nitrogen protection (Supporting Information Fig. S2A and B). The successful synthesis of ODex and Gel−NO were confirmed by ^{1}H NMR hydrogen spectroscopy. The characteristic proton signal at 5.00 ppm is the evidence for the synthesis of Gel−NO (Fig. 1A). The successful synthesis of ODex was evidenced by a distinctive peak at 8.31 ppm (Fig. 1B). Concurrently, PF127 was reacted with carboxylic acid phenylboronic acid under a catalytic system of EDC/DMAP and under nitrogen protection to form PF127BA (Supporting Information Fig. S2C). The characteristic peak at 7.63 ppm indicated the successful synthesis of PF127BA (Fig. 1C). Due to the hydrophobicity of ISO-1, ISO-1 was encapsulated within PF127BA nanoparticles using the thin-film hydration method[34]. The size and shape of the nanoparticles were measured using DLS and TEM. The size of PF127BA and PF127B@ISO-1 nanoparticles was shown in Fig. 1D, with average diameters of 101.33 nm and 79.29 nm, respectively. The particle size of drug-loaded nanoparticles is slightly smaller than that of blank nanoparticles, which may be attributed to the increased density of the nanoparticles upon drug loading. This enhancement in density could facilitate the aggregation of nanoparticles during the fabrication process, resulting in reduced particle size[35]. The diminished particle diameter potentially augments their diffusivity and penetrating capability within biological systems. TEM images showed that both PF127BA and PF127B@ISO-1 nanoparticles are uniformly sized spherical particles (Fig. 1E). The sol-gel transition was demonstrated using the inverted vial method, and the injectability of the hydrogel was observed by injecting it with a syringe, indicating that the synthesized hydrogel has good gelation and injectability (Fig. 1F). The internal fracture structure of the three freeze-dried hydrogels was captured using SEM, showing similar structural information with honeycomb-like pores of similar sizes (Fig. 1G). Frequency sweep results showed that within the frequency range of 0.1−100 rad/s, the storage modulus (G') is always greater than the loss modulus (G''), indicating the gel state under test conditions (Fig. 1H). The modulus of the hydrogel at 1−2 kPa is comparable to that of the mouse cerebral cortex[36]. To determine the ISO-1 release efficiency under physiological and pathological conditions, tests were conducted in PBS pH = 7.4 and PBS pH = 6.5 with 1 mmol/L H_2O_2, respectively. The drug loading of ISO-1 NPs was 43.87 ± 4.04%. The degree substitution of NO donor was determined to be 29.89%. The release curve shows that the final release rate of ISO-1 in G_{NO}−OD HG@ISO-1 NPs in PBS pH = 7.4 after 14 days is 54.67%, while in PBS pH = 6.5 with 1 mmol/L H_2O_2, the final release rate is 70.69% (Fig. 1I). It can be observed that the release of ISO-1 conforms more closely to the first-order rate model under both conditions (Supporting Information Table S1). Thus, it can be seen that the release efficiency of ISO-1 in an inflammatory microenvironment is higher than in a physiological environment. Similarly, the release of NO was also monitored, with Fig. 1J showing the release of NO from the G_{NO}−OD HG@ISO-1 NPs hydrogel. Similar to the release of ISO-1, the cumulative concentration of NO released under the condition of PBS pH = 6.5 with 1 mmol/L H_2O_2 is higher than in PBS pH = 7.4. This is attributed to the rapid degradation of the hydrogel under the inflammatory microenvironment. Under the condition of PBS pH = 6.5 with 1 mmol/L H_2O_2, the cumulative concentration of NO released on the 14th day is 42.54 μmol/L, while in PBS pH = 7.4, the cumulative concentration is 33.65 μmol/L (Fig. 1J). The condition of PBS pH = 6.5 with 1 mmol/L H_2O_2 is similar to the pathological microenvironment after cerebral infarction, indicating that injecting the hydrogel designed in this study into the infarction area has good drug release efficiency and a modulus that matches the rat cerebral cortex, making it feasible for *in situ* injection in the stroke cavity[37].

3.2. *Anti-apoptotic and anti-inflammatory effects*

To investigate the potential influence of the hydrogel on ischemic injury, we established an OGD model using HT22 and BV2 cell lines to simulate ischemic damage. The three types of hydrogels were co-cultured with HT22-/-BV2 cells for 48 h, then the cell compatibility and metabolic activity in HT22 and BV2 cells were assessed using CCK-8 and live/dead staining and utilizing the 2′,7′−dichlorodihydrofluorescein diacetate (DCFH-DA) probe method to quantify the ROS content within cells (Fig. 2A−E). The live/dead cell staining results showed that after 48 h of co-culture with G_{NO}−OD HG, G_{NO}−OD HG@ NPs, and G_{NO}−OD HG@ISO-1 NPs, the group co-cultured with G_{NO}−OD HG@ISO-1 NPs had a higher number of live cells and fewer dead cells for both HT22 and BV2 cells, indicating that the hydrogels have good cell compatibility and proliferative capacity (Fig. 2A and B). In terms of cell viability, the HT22 cell viability in the OGD group decreased to 47.66%, and the BV2 cell viability decreased to 59.79%. After 48 h of co-culture with G_{NO}−OD HG, G_{NO}−OD

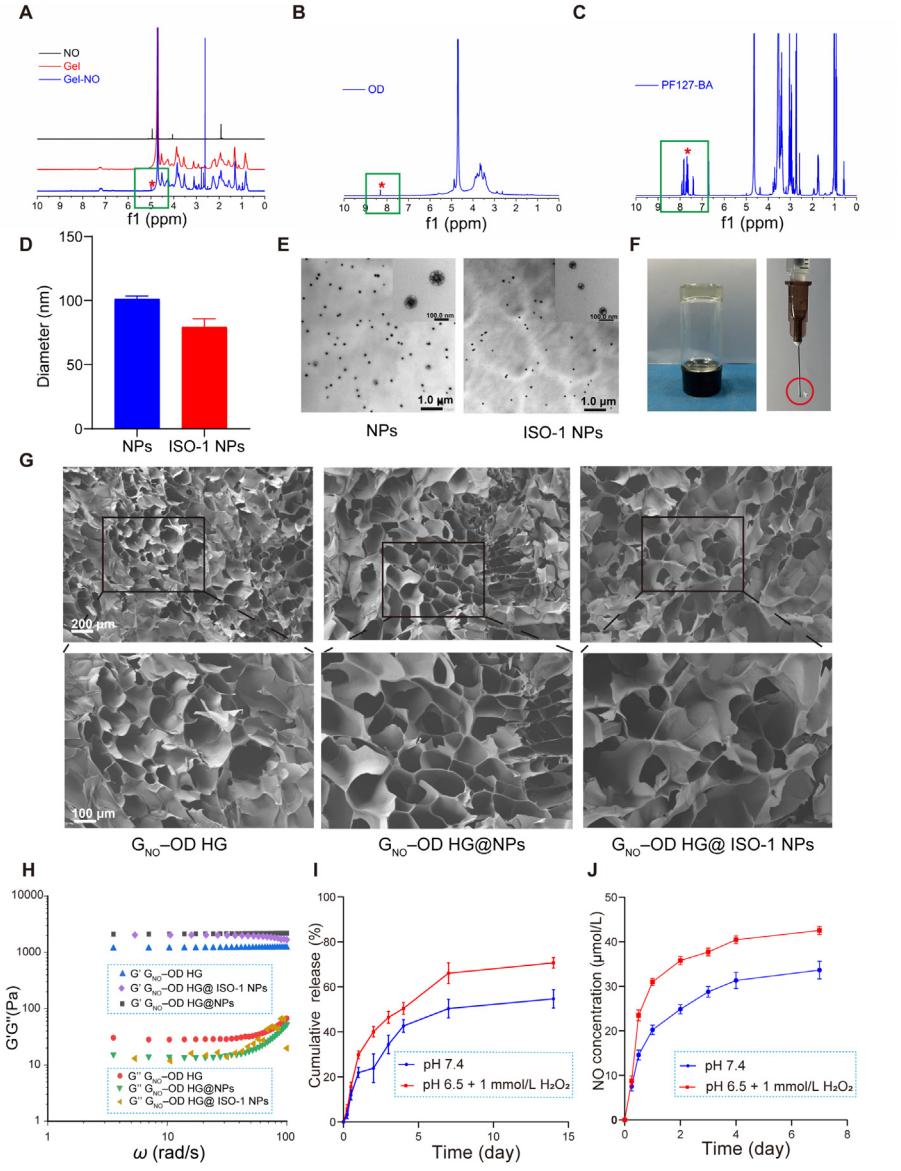

Figure 1 Synthesis, characterization, and *in vitro* drug release of hydrogels and nanoparticles. (A) The ^{1}H NMR spectra of NO, Gel, and Gel−NO. (B) The ^{1}H NMR spectra of OD. (C) The ^{1}H NMR spectra of PF127-BA. (D) The DLS data of the nanoparticles. (E) The TEM images of NPs and ISO-1 NPs. (F) The sol-gel transition of the hydrogels and photos of hydrogel (G_{NO}−OD HG@ISO-1 NPs) were being injected. (G) The SEM images of G_{NO}−OD HG, G_{NO}−OD HG@ NPs, and G_{NO}−OD HG@ISO-1 NPs. (H) The results of rheological tests of hydrogel. (I,J) The *in vitro* cumulative release profile of ISO-1 and concentration of NO from G_{NO}−OD HG@ISO-1 NPs in pH 7.4 and pH 6.5 with 1 mmol/L H_2O_2 (data are presented as mean ± SD, $n = 3$).

HG@ NPs, and G_{NO}−OD HG@ISO-1 NPs, the HT22 cell viability showed a significant improvement compared to the OGD group, with 52.74%, 60.96%, and 88.64%, respectively. The BV2 cell viability also showed a significant improvement compared to the OGD group, with 65.58%, 71.90%, and 79.04%, respectively (Fig. 2C and D). This suggested that these hydrogels had good cell compatibility and could improve the activity of HT22 and BV2 affected by OGD.

ROS are primarily produced due to the ischemic and glucose-deprived environment that simulates ischemic stroke, leading to energy metabolism imbalance, and ROS are also one of the mechanisms that further affect the progression of ischemic stroke[38]. DCFH-DA is a probe that can detect ROS, exhibiting green fluorescence. DCFH-DA staining results showed significant green fluorescence in the OGD group, indicating a large amount of ROS production. However, in the co-culture with HT22 and BV2 cells and G_{NO}−OD HG, G_{NO}−OD HG@ NPs, and G_{NO}−OD HG@ISO-1 NPs, there was a decrease in both the number of ROS and fluorescence intensity, indicating that the hydrogel had some scavenging effect on ROS induced by OGD (Fig. 2D and E).

To explore the hydrogel's effect on controlling inflammation, we co-cultured G_{NO}−OD HG, G_{NO}−OD HG@ NPs, and G_{NO}−OD HG@ISO-1 NPs with BV2 cells for 48 h. We examined the expression of MIF, which is specifically inhibited by ISO-1, and found that G_{NO}−OD HG and G_{NO}−OD HG@ NPs showed a decrease compared to the OGD group, while the G_{NO}−OD HG@ISO-1 NPs group showed a significant decrease, with MIF levels approaching those of the normal control group (Fig. 2F).

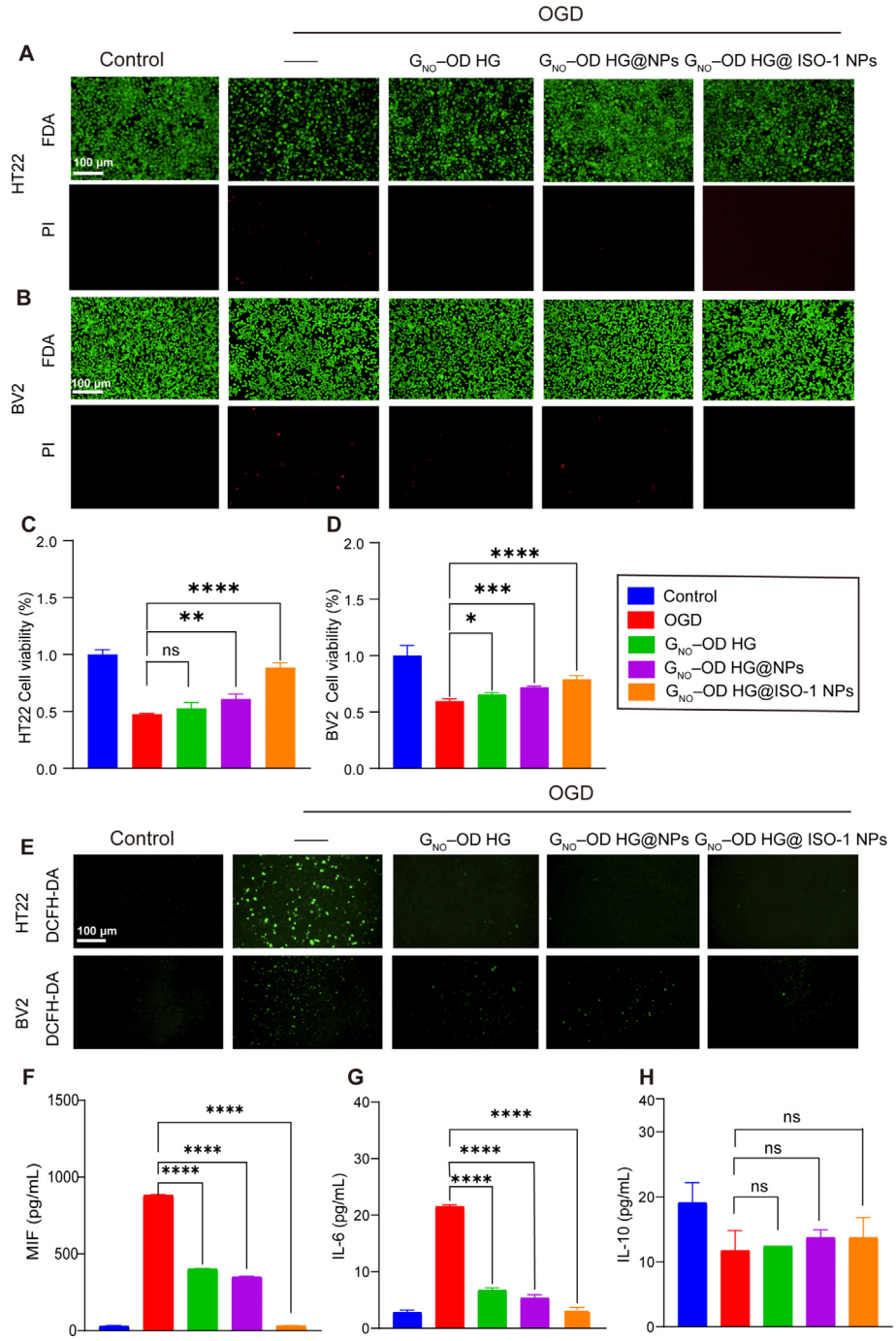

Figure 2 Cellular biocompatibility and expression of inflammatory cytokines *in vitro*. (A, B) Representative images of FDA/PI (live/dead) staining for HT22 cells and BV2 with different hydrogels. (C, D) CCK-8 assay for HT22 and BV2 cells treated with different hydrogels. (E) Representative images of DCFH-DA (ROS) staining for HT22 and BV2. (F−H) ELISA quantitative assay of MIF, IL-6 and IL-10 in BV2 cells with different treatments. $^{*}P < 0.05$, $^{**}P < 0.01$, $^{***}P < 0.001$, $^{****}P < 0.0001$, ns, not significant (mean ± SD, $n = 3$), scale bar = 100 μm.

Additionally, the expression levels of IL-6 were measured and found to have decreased in all three hydrogel treatment groups compared to the OGD group. We also examined the level of IL-10 and found that the expression level of IL-10 was increased, but not statistically significant (Fig. 2G and H). This indicates that the hydrogel has a good anti-inflammatory effect, and G_{NO}−OD HG@ISO-1 NPs can specifically inhibit MIF, while the decrease in MIF in other hydrogels may be due to their universal anti-inflammatory effect[39-41].

3.3. *Hydrogel's anti-inflammatory, antioxidant, angiogenic, and neuroprotective effects post-cerebral ischemic injury*

We established a PT stroke model in mice to explore the *in vivo* therapeutic effects of the hydrogel on ischemic injury. 3 days after the model establishment, different hydrogels or saline were injected *via* a stereotactic apparatus into the brain. The specific experimental route of animal studies in this research is shown in

Fig. 3A. Mice were randomly divided into 5 groups: sham operation group (sham), saline-injected post-stroke group (PT group), G_{NO}−OD HG-injected post-stroke group (G_{NO}−OD HG), G_{NO}−OD HG@ NPs-injected post-stroke group (G_{NO}−OD HG@ NPs), and G_{NO}−OD HG@ISO-1 NPs-injected post-stroke group (G_{NO}−OD HG@ISO-1 NPs). To verify the success of the model, we observed the PT and sham groups of mice through hematoxylin and eosin (H&E) staining. We found that under H&E staining, the PT group exhibited numerous cellular vacuoles and shrunken nuclei, indicating the presence of infarcts (Supporting Information Fig. S3).

To further explore the underlying mechanisms, we focused on anti-inflammatory, angiogenic, and neuroprotective pathways, detecting relevant proteins at corresponding time points through immunofluorescence (IF). During the first week, we assessed apoptosis in brain tissue cells using TUNEL expression (Fig. 3B). Compared to the sham group, the number of TUNEL-positive cells significantly increased in the PT group (0.12 ± 0.21 *vs.* 7.50 ± 1.29, $P < 0.001$), and after treatment with G_{NO}−OD HG, G_{NO}−OD HG@ NPs, and G_{NO}−OD HG@ISO-1 NPs, the number of TUNEL-positive cells decreased compared to the PT group

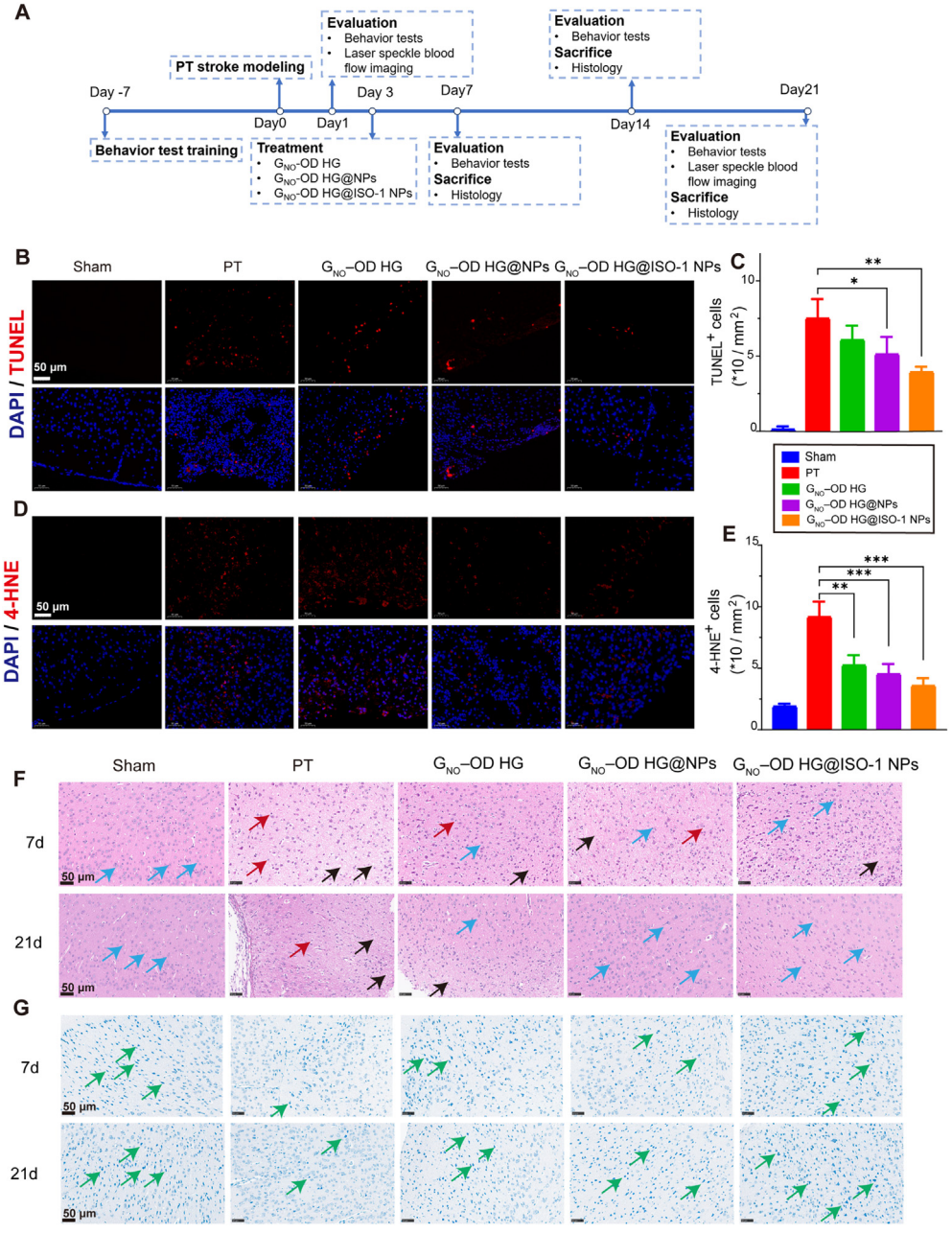

Figure 3 *In vivo* anti-apoptotic and antioxidant efficacy of G_{NO}−OD HG@ISO-1 NPs. (A) The timeline of animal experiments. (B, C) Representative immunofluorescent (IF) staining image of TUNEL and quantitative analysis of TUNEL-positive cells. (D, E) Representative IF staining image of 4-HNE and quantitative analysis of 4-HNE-positive cells. (F,G) H&E staining and Nissl staining in the sham, PT, and various treatment groups. Blue arrows indicate normal neuronal cells, red arrows point to shrunken neuronal cells post-stroke, black arrows denote vacuoles formed after stroke, and green arrows highlight neurons with Nissl bodies. The nucleus was labeled with DAPI. $^{*}P < 0.05$, $^{**}P < 0.01$, $^{***}P < 0.001$ (mean ± SD, $n = 3$), scale bar = 50 μm.

(6.07 ± 0.94, 5.12 ± 1.15, 3.93 ± 0.36), shown in Fig. 3C. Additionally, we examined 4-hydroxynonenal (4-HNE), a highly toxic lipid peroxidation end product associated with ferroptosis[37]. The results showed a significant increase in 4-HNE levels in the PT group compared to the sham group (9.17 ± 1.25 *vs.* 1.91 ± 0.21, $P < 0.001$). After treatment with G_{NO}−OD HG (5.24 ± 0.82), G_{NO}−OD HG@ NPs (4.52 ± 0.82), and G_{NO}−OD HG@ISO-1 NPs (3.57 ± 0.62), the number of 4-HNE-positive cells significantly decreased, especially in the G_{NO}−OD HG@ISO-1 NPs group (Fig. 3D and E). This suggested that NO and ISO-1 exert neuroprotective and antioxidant effects, inhibiting neuronal apoptosis and oxidation to a certain extent[42,43].

Consequently, we performed H&E staining and Nissl body staining on mouse brain sections at 7 and 21 days post-modeling. According to our experimental results, in H&E staining, it can be observed that on Day 7, during the early phase of cerebral infarction, compared to the PT group, the brain tissue exhibited cortical neuronal cell shrinkage, visible necrotic neurons, a reduction in the neuronal count, and vacuole formation between tissues (Fig. 3F). In contrast, the treatment groups showed milder neuronal damage. By Day 21, the ischemic injury in the PT group's brain tissue had alleviated compared to Day 7. On Day 21, ischemic injuries in all treatment groups had also significantly improved, especially in the G_{NO}−OD HG@ISO-1 NPs group.

Regarding neuronal restoration, Nissl body staining revealed that on Day 7, compared to the sham group, the PT group exhibited a reduction in the number of Nissl bodies in the cerebral cortex, with deeply stained and condensed nuclei and disordered arrangement. In the treatment groups, however, the number of Nissl bodies increased (Fig. 3G). By Day 21, there was a slight recovery in the morphology and quantity of Nissl bodies in the PT group, but there was still a significant difference compared to the sham group. The treatment groups showed a marked increase in the number of Nissl bodies compared to Day 7 and were greater than those in the PT group.

In the second week of treatment, we assessed the inflammatory level by observing proteins such as CD86, CD206, MIF, MMP-9, IL-6 and IL-10 (Fig. 4 and Supporting Information Fig. S4). CD86 and CD206 are surface-specific markers of the activated microglial M1 pro-inflammatory phenotype and M2 anti-inflammatory phenotype, respectively[44,45]. IF results showed that the number of CD86 and CD206 positive cells significantly increased in the PT group compared to the sham group, and after treatment with G_{NO}−OD HG, G_{NO}−OD HG@ NPs, and G_{NO}−OD HG@ISO-1 NPs, both CD86 and CD206 significantly decreased compared to the PT group, especially in the G_{NO}−OD HG@ISO-1 NPs treatment group (Fig. 4A, B, G and J). In the PT, G_{NO}−OD HG, G_{NO}−OD HG@NPs, and G_{NO}−OD HG@ISO-1 NPs groups, the numbers of CD86 protein-positive cells were 6.19 ± 0.74,

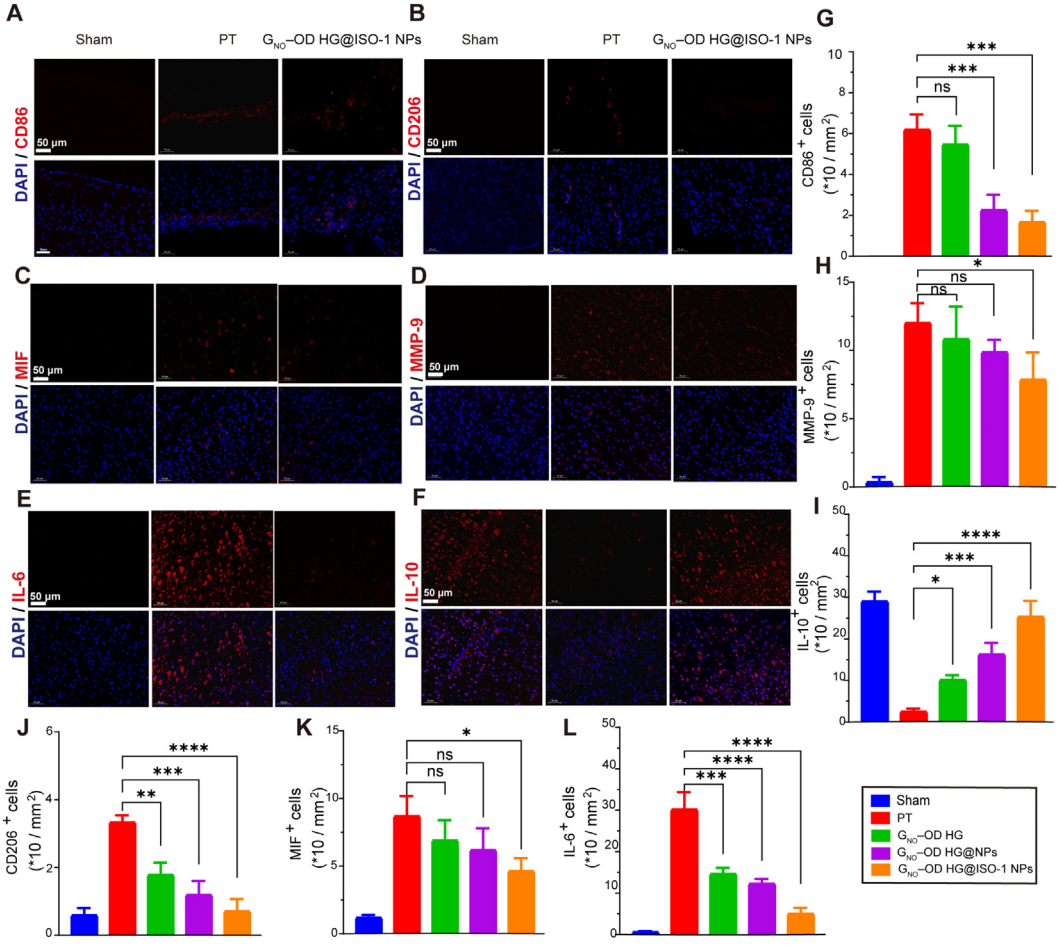

Figure 4 *In vivo* anti-inflammation efficacy of G_{NO}−OD HG@ISO-1 NPs. (A−F) Representative IF staining of CD86, CD206, MIF, MMP-9, IL-6 and IL-10. The nucleus was labeled with DAPI. (G−L) Quantitative analyses of CD86-positive, MMP-9-positive, IL-10-positive, CD206-positive, MIF-positive and IL-6-positive cells. *$P < 0.05$, **$P < 0.01$, ***$P < 0.001$, ns, not significant (mean ± SD, $n = 3$), scale bar = 50 μm.

5.48 ± 0.90, 2.26 ± 0.74, and 1.67 ± 0.55, respectively. And, the numbers of CD206 protein-positive cells were 3.33 ± 0.21, 1.79 ± 0.36, 1.19 ± 0.41, and 0.71 ± 0.36, respectively. These results indicated a significant modulation of the immune response as evidenced by the expression of the CD86 and CD206 co-stimulatory molecules. This indicated that NO and ISO-1 exhibited excellent anti-inflammatory effects. Similarly, the expression of MIF and MMP-9 also decreased in the treatment groups with G_{NO}−OD HG, G_{NO}−OD HG@ NPs, and G_{NO}−OD HG@ISO-1 NPs, with the most significant decrease in the G_{NO}−OD HG@ISO-1 NPs group. In the PT, G_{NO}−OD HG, G_{NO}−OD HG@NPs, and G_{NO}−OD HG@ISO-1 NPs groups, the numbers of MIF protein-positive cells were 8.69 ± 1.49, 6.91 ± 1.49, 6.19 ± 1.61, and 4.64 ± 0.94, respectively. And, the numbers of MMP-9 protein-positive cells were 12.02 ± 1.44, 10.83 ± 2.38, 9.88 ± 0.90, and 7.86 ± 1.99, respectively (Fig. 4C, D, H and K). This suggested that G_{NO}−OD HG@ISO-1 NPs had a more pronounced specific inhibitory effect on MIF and MMP-9. To corroborate the results of the protein content of IL-6 and IL-10 detected in cell experiments, we observed the expression of these two proteins in mouse brain sections through IF staining. The results were consistent with the cell experiments, showing that the protein expression of IL-6 (Fig. 4E and L) in the brain sections of mice with cerebral infarction was higher compared to the sham group, while the expression of IL-6 in the three treated groups decreased. Conversely, compared to the sham group, the expression of IL-10 (Fig. 4F and I) was lower in the PT group, and the expression of IL-10 in the three treated groups was higher than in the PT group, especially in the G_{NO}−OD HG@ISO-1 NPs group.

In the third week of treatment, we further assessed the proteins related to angiogenesis, CD31, α-SMA, eNOS, PDGFR, and VEGF (Fig. 5 and Supporting Information Fig. S5). In the PT, G_{NO}−OD HG, G_{NO}−OD HG@NPs, and G_{NO}−OD HG@ISO-1 NPs groups, the numbers of CD31 protein-positive cells were 11.90 ± 1.25, 13.33 ± 1.35, 14.17 ± 3.08, and 14.64 ± 2.50, respectively. In the PT, G_{NO}−OD HG, G_{NO}−OD HG@NPs, and G_{NO}−OD HG@ISO-1 NPs groups, the numbers of α-SMA protein-positive cells were 3.45 ± 0.90, 5.60 ± 0.21, 6.43 ± 1.29, and 7.02 ± 1.49, respectively. It can be observed that the levels of these two proteins increased in the treatment groups with G_{NO}−OD HG, G_{NO}−OD HG@ NPs, and

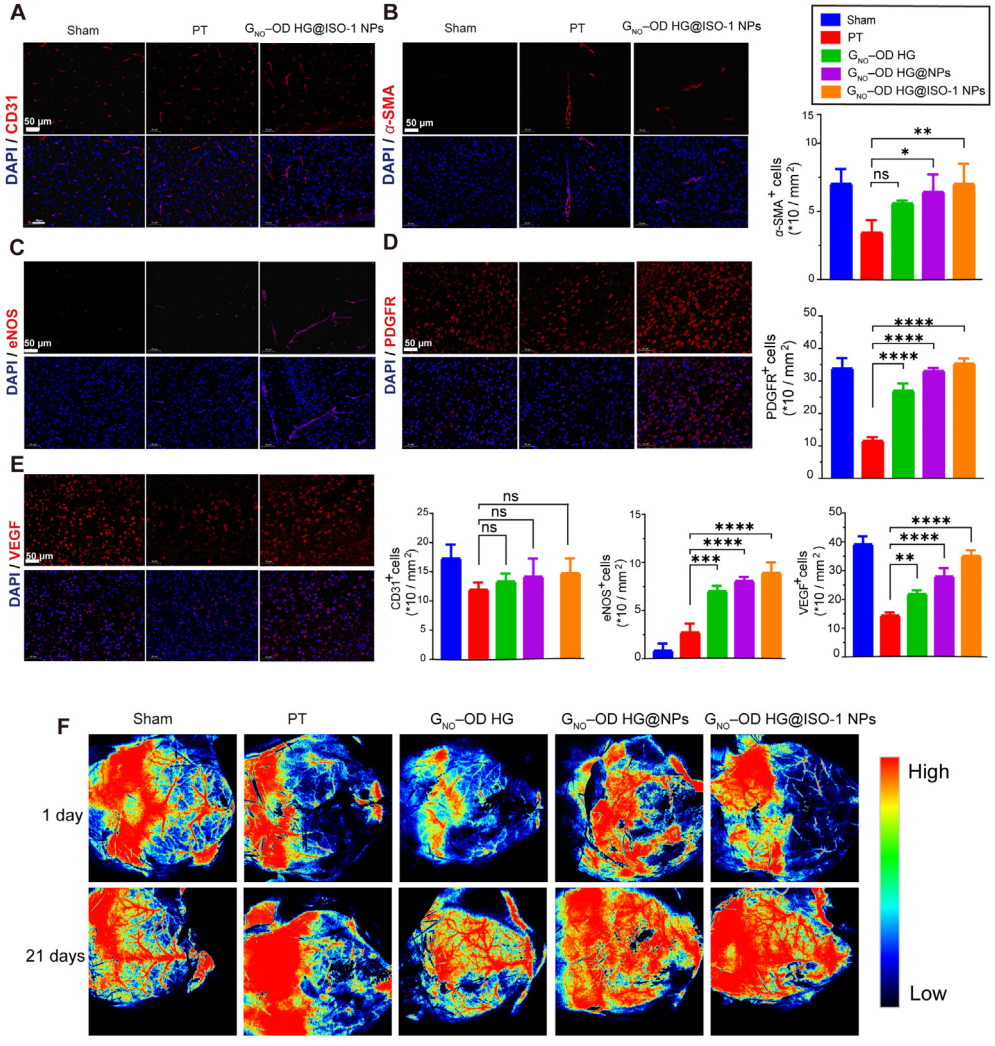

Figure 5 *In vivo* efficacy in promoting angiogenesis of G_{NO}−OD HG@ISO-1 NPs. (A−E) Representative IF staining and quantitative analysis of CD31, α-SMA, eNOS, PDGFR, and VEGF. The nucleus was labeled with DAPI. (F) The representative image of laser speckle blood flow in different treatments. *$P < 0.05$. **$P < 0.01$. *** $P < 0.001$. ns, not significant, (mean ± SD, $n = 3$), scale bar = 50 μm.

G_{NO}−OD HG@ISO-1 NPs (Fig. 5A and B), indicating that the designed hydrogels can promote angiogenesis during the third week. We also detected the expression of endothelial nitric oxide synthase (eNOS, Fig. 5C), platelet-derived growth factor receptor (PDGFR, Fig. 5D), and vascular endothelial growth factor (VEGF, Fig. 5E) and found that all three proteins were highly expressed in the G_{NO}−OD HG@ISO-1 NPs group. eNOS is an enzyme expressed in vascular endothelial cells that catalyzes the conversion of L-arginine to NO. The NO produced by eNOS can increase vascular relaxation, thereby improving cerebral blood flow, which has a positive effect on the recovery of blood flow in the infarcted area. During the repair process after cerebral infarction, eNOS may be involved in promoting new blood vessel formation, helping to restore blood supply to damaged brain tissue. In cerebral infarction, eNOS may also interact with inflammatory cytokines such as IL-6, affecting inflammatory responses and cellular damage. PDGFR mainly plays a role in the proliferation and migration of vascular smooth muscle cells and pericytes, contributing to vascular reconstruction and repair after cerebral infarction. VEGF is a group of signaling proteins with angiogenic effects, playing a key role in neovascularization, vascular repair, and vascular maintenance. The increase in these three proteins in the G_{NO}−OD HG@ISO-1 NPs group indicates that hydrogel treatment promotes the process of angiogenesis.

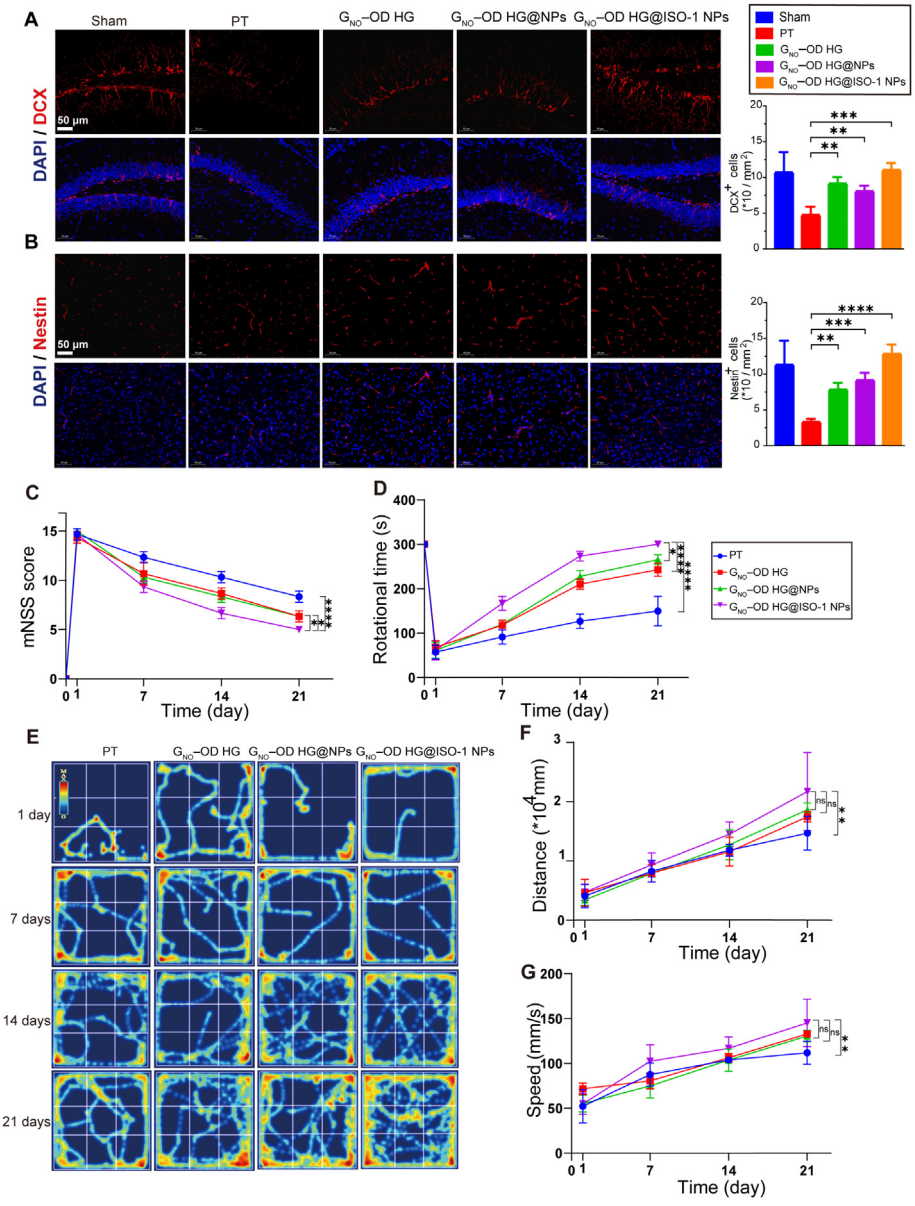

Figure 6 *In vivo* efficacy in nerve and protection behavioral assessment in animals. Representative IF staining image of DCX and quantitative analysis of DCX-positive cells (A, B). Representative IF staining image of Nestin and quantitative analysis of Nestin-positive cells. The nucleus was labeled with DAPI. (C) The mNSS score of mice in different groups was recorded every 7 days ($n = 5$). (D) The stay time of mice until fall from the rotated apparatus in the rotarod test ($n = 5$). (E) The movement trajectories of different groups in the open field. (F, G) The movement distance and speed of different groups in the open field test. $^*P < 0.05$. $^{**}P < 0.01$. $^{***}P < 0.001$. $^{****}P < 0.0001$. ns, not significant (mean ± SD, $n = 3$), scale bar = 50 μm.

Therefore, *in vivo*, we used a laser speckle blood flow imager to observe cerebral ischemia and angiogenesis, on the first day after modeling, compared to the sham group, other groups showed significant cerebral ischemic areas with obvious vascular damage. On the Day 21 after modeling, compared to Day 1, the cerebral ischemic areas decreased in all groups, while the PT group showed less reduction, with a large part of the ischemic area still present, while the treatment groups G_{NO}−OD HG, G_{NO}−OD HG@ NPs, and G_{NO}−OD HG@ISO-1 NPs showed a significant improvement in cerebral ischemia and re-established a rich blood supply (Fig. 5F). These results indicate that treatment of cerebral infarction *via* the designed hydrogel can promote angiogenesis and reestablish blood perfusion. Such effects are also conducive to the recovery of neurological function in the later stages of cerebral infarction[46-48].

In terms of neuroprotection, we examined the expression of doublecortin (DCX, Fig. 6A) and Nestin (Fig. 6B) and found that both were highly expressed in the G_{NO}−OD HG@ISO-1 NPs group. DCX is a protein associated with microtubules and plays an important role in neuronal migration and plasticity. DCX helps in the reorganization and functional recovery of damaged neural networks, protecting neurons from cell death caused by ischemic injury. Nestin is an intermediate filament protein expressed in neural stem cells and progenitor cells. The upregulation of Nestin is usually associated with the activation and proliferation of neural precursor cells, which can differentiate into neurons and glial cells, participating in the process of neural regeneration and repair after cerebral infarction. Nestin is also expressed in vascular endothelial cells and during angiogenesis, especially in the formation of new blood vessels. Nestin-positive cells may be involved in the vascular reconstruction of the infarcted area, helping to improve blood flow in damaged brain tissue. This indicates that after hydrogel treatment, the related processes of neural regeneration and repair in mice were activated.

3.4. *Neurological functional recovery*

Neurological functional recovery analyses included mNSS, rotarod test, and open field test. Neurological functions were dynamically monitored from before surgery to 3 weeks after hydrogel injection. The mNSS score is a comprehensive assessment that includes motor, sensory, reflex, and balance functions[49]. The lower the score is, the better the neurological function of mice. After the model establishment, there was a significant neurological deficit in mice, which began to recover after treatment with G_{NO}−ODHG, G_{NO}−OD HG@ NPs, and G_{NO}−OD HG@ISO-1 NPs (Fig. 6C). On Day 21, the G_{NO}−OD HG@ISO-1 NPs treatment group showed the best recovery of neurological function, with a significant difference from the PT group. The rotarod test measures the time mice can stay on a rotating rod, with a longer duration indicating better neurological function[50]. On Day 21, the G_{NO}−OD HG@ISO-1 NPs treatment group had the longest duration on the rotarod, indicating the best recovery of neurological function (Fig. 6D). Finally, the open field test was conducted to assess the spontaneous behavioral and exploratory abilities of mice with ischemic stroke[51]. Fig. 6E recorded the movement trajectories of different groups in the field. Compared to the PT group, the G_{NO}−OD HG@ISO-1 NPs group showed a significant increase in movement distance (Fig. 6F) and movement speed (Fig. 6G), which means the mice's spontaneous movement and exploratory abilities were substantially improved. The other two groups (G_{NO}−OD HG and G_{NO}−OD HG@ NPs) also showed improved spontaneous movement abilities compared to the PT group. In summary, the neurological deficits in mice were partially recovered after treatment with G_{NO}−OD HG, G_{NO}−OD HG@ NPs, and G_{NO}−OD HG@ISO-1 NPs, especially in the G_{NO}−OD HG@ISO-1 NPs group, indicating that NO and ISO-1 significantly contributed to the recovery of neurological function.

3.5. *Transcriptome sequencing*

On Day 21 post-treatment, brain tissue from the cerebral infarction area was harvested for mRNA sequencing. The gene expression profiles of the PT group and the composite hydrogel group (G_{NO}−OD HG@ISO-1 NPs) were analyzed to assess the effects of NO and ISO-1 at the genetic level. As shown in the figure, there were 375 differentially expressed genes between these two groups, with 241 upregulated and 134 downregulated (Supporting Information Fig. S6). The Kyoto Encyclopedia of Genes and Genomes (KEGG) database was used for enrichment pathway analysis. The inflammation and immune-related pathways included Th1 and Th2 cell differentiation, viral protein interaction with cytokine and cytokine receptor, Th17 cell differentiation, TNF signaling pathway, antigen processing and presentation, cytokine-cytokine receptor interaction, chemokine signaling pathway, and cell adhesion molecules. Neurological function-related pathways included the dopaminergic synapse and neuroactive ligand-receptor interaction (Supporting Information

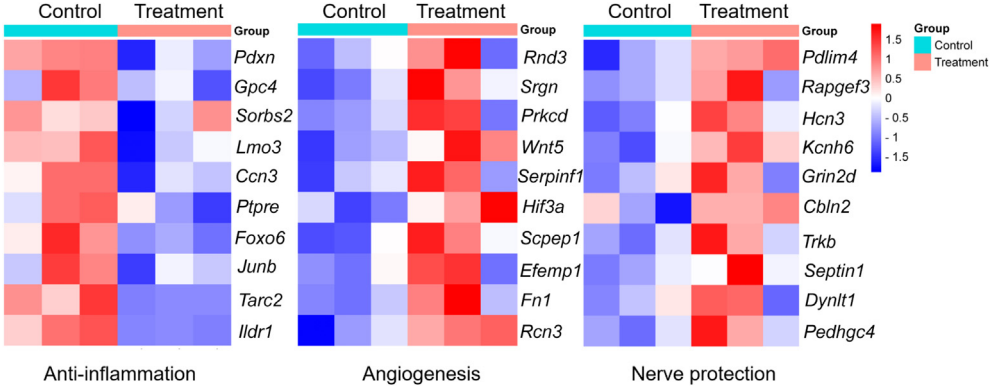

Figure 7 Transcriptomic heat map analysis of genes related to anti-inflammation, angiogenesis, and nerve protection functions.

Fig. S7A). The KEGG classification showed that the differentially expressed genes were enriched in pathways related to cellular processes, environmental information processes, human diseases, metabolism, and organ systems (Fig. S7B). Some regulated genes were involved in various GO terms, such as chemokine activity, response to interferon-gamma and interferon-beta, Major histocompatibility complex (MHC) and MHC class II protein complex binding, and neurotransmitter transport (Fig. S7C). The differentially expressed genes were enriched in many GO terms, categorized as biological process (BP), cellular component (CC), and molecular function (MF) (Fig. S7D). These results indicated G_{NO}−OD HG@ISO-1 NPs exerted multiple functions to improve ischemic injury. We conducted an analysis of specific genes related to mechanisms such as angiogenesis, anti-inflammation, and neuroprotection using transcriptomic data. We found that some genes were highly expressed in the treatment group (Fig. 7). However, due to the limitation of sample size, the results obtained still require further validation.

4. Conclusions

In summary, we have constructed an *in situ* hydrogel platform with excellent biocompatibility for the sustained release of NO and ISO-1, targeting multiple pathogenic mechanisms such as anti-inflammation, angiogenesis promotion, and antioxidant effects post-stroke, showing promising therapeutic prospects. The performance characterization of the hydrogel demonstrated that the multifunctional hydrogel possesses excellent injectability and intelligent drug release capabilities. Cellular experimental results indicated that the hydrogel platform possesses good biocompatibility and is capable of scavenging ROS and inflammation-related cytokines such as IL-6, IL-10, and MIF. In a mouse model of ischemic stroke, the multifunctional hydrogel inhibited inflammation, rescued apoptotic neurons, and promoted angiogenesis. Furthermore, assessments through the mNSS, rotarod test, and open field test demonstrated that the hydrogel significantly improved the motor functional deficits in mice after cerebral ischemic injury in the long-term therapeutic effect. In conclusion, we have designed a multifunctional hydrogel that responds to the pathological microenvironment of the brain, capable of sustained release of NO and ISO-1, thereby alleviating cerebral ischemic injury.

Acknowledgments

This study was supported by the funding listed as follows: National Key R&D Program of China (Nos. 2018YFC2002100 and 2018YFC2002103), Science and Technology Department of Sichuan Province (Grant No. 24ZYZYTS0172 and 2025ZNSFSC1021, China), the Key R&D Support Program of Chengdu (No. 2022YF0900001SN, China), National Natural Science Foundation of China (No. 32301115), National Key Research and Development Programs (2023YFC2412802, China), and Fundamental Research Funds for the Central Universities (2023SCUH0011 and YJ2021115, China). Thanks for advise of Chong Chen.

Author contributions

Wen Guo: Writing − original draft, Methodology, Data curation. Cheng Hu: Project administration, Methodology, Funding acquisition, Conceptualization. Yue Wang: Formal analysis, Data curation. Wen Zhang: Methodology, Data curation. Shaomin Zhang: Supervision. Jin Peng: Formal analysis. Yunbing Wang: Writing − review & editing, Visualization, Funding acquisition. Jinhui Wu: Writing − review & editing, Methodology, Funding acquisition, Conceptualization.

Conflicts of interest

The authors declare no conflicts of interest.

Appendix A. Supporting information

Supporting information to this article can be found online at https://doi.org/10.1016/j.apsb.2025.01.005.

References

1. Wu SM, Wu B, Liu M, Chen ZM, Wang WZ, Anderson CS, et al. Stroke in China: advances and challenges in epidemiology, prevention, and management. *Lancet Neurol* 2019;**18**:394−405.
2. Feigin VL, Brainin M, Norrving B, Martins S, Sacco RL, Hacke W, et al. World Stroke Organization (WSO): global stroke fact sheet 2022. *Int J Stroke* 2022;**17**:18−29.
3. Tsao CW, Aday AW, Almarzooq ZI, Anderson CAM, Arora P, Avery CL, et al. Heart disease and stroke statistics-2023 update: a report from the American Heart Association. *Circulation* 2023;**147**:E93−621.
4. Hilkens NA, Casolla B, Leung TW, de Leeuw FE. Stroke. *Lancet* 2024;**403**:2820−36.
5. D'Apolito E, Sisalli MJ, Tufano M, Annunziato L, Scorziello A. Oxidative metabolism in brain ischemia and preconditioning: two sides of the same coin. *Antioxidants (Basel)* 2024;**13**:547.
6. Zhang Y, Zhang HY, Zhao FQ, Jiang ZP, Cui YL, Ou MT, et al. Mitochondrial-targeted and ROS-responsive nanocarrier *via* nose-to-brain pathway for ischemic stroke treatment. *Acta Pharm Sin B* 2023;**13**:5107−20.
7. Ramos-Mondragón R, Lozhkin A, Vendrov AE, Runge MS, Isom LL, Madamanchi NR. NADPH oxidases and oxidative stress in the pathogenesis of atrial fibrillation. *Antioxidants (Basel)* 2023;**12**:1833.
8. Guo BA, Yang FY, Zhang LP, Zhao QX, Wang WK, Yin L, et al. Cuproptosis induced by ROS responsive nanoparticles with elesclomol and copper combined with αPD-L1 for enhanced cancer immunotherapy. *Adv Mater* 2023;**35**:e2212267.
9. Muhammad W, Zhu JQ, Zhai ZH, Xie JQ, Zhou JH, Feng XD, et al. ROS-responsive polymer nanoparticles with enhanced loading of dexamethasone effectively modulate the lung injury microenvironment. *Acta Biomater* 2022;**148**:258−70.
10. Ding HT, Tan P, Fu SQ, Tian XH, Zhang H, Ma XL, et al. Preparation and application of pH-responsive drug delivery systems. *J Control Release* 2022;**348**:206−38.
11. Tsivgoulis G, Katsanos AH, Sandset EC, Turc G, Nguyen TN, Bivard A, et al. Thrombolysis for acute ischaemic stroke: current status and future perspectives. *Lancet Neurol* 2023;**22**:418−29.
12. Paul S, Candelario-Jalil E. Emerging neuroprotective strategies for the treatment of ischemic stroke: an overview of clinical and preclinical studies. *Exp Neurol* 2021;**335**:113518.
13. Li C, Sun T, Jiang C. Recent advances in nanomedicines for the treatment of ischemic stroke. *Acta Pharm Sin B* 2021;**11**:1767−88.
14. Ruan HT, Li YF, Wang C, Jiang YX, Han YL, Li YW, et al. Click chemistry extracellular vesicle/peptide/chemokine nanocarriers for treating central nervous system injuries. *Acta Pharm Sin B* 2023;**13**:2202−18.
15. Chatterjee S, Chi-Leung Hui P. Review of stimuli-responsive polymers in drug delivery and textile application. *Molecules* 2019;**24**:2547.
16. Madai S, Kilic P, Schmidt R, Bas-Orth C, Korff T, Büttner M, et al. Activation of the hypoxia-inducible factor pathway protects against

acute ischemic stroke by reprogramming central carbon metabolism. *Theranostics* 2024;**14**:2856−80.
17. Li N, Ren CH, Li SJ, Yu WT, Jin KL, Ji XM. Remote ischemic conditioning alleviates chronic cerebral hypoperfusion-induced cognitive decline and synaptic dysfunction *via* the miR-218a-5p/SHANK2 pathway. *Prog Neurobiol* 2023;**230**:102514.
18. Xin WQ, Pan YL, Wei W, Tatenhorst L, Graf I, Popa-Wagner A, et al. Preconditioned extracellular vesicles from hypoxic microglia reduce poststroke AQP4 depolarization, disturbed cerebrospinal fluid flow, astrogliosis, and neuroinflammation. *Theranostics* 2023;**13**:4197−216.
19. Maida CD, Norrito RL, Daidone M, Tuttolomondo A, Pinto A. Neuroinflammatory mechanisms in ischemic stroke: focus on cardioembolic stroke, background, and therapeutic approaches. *Int J Mol Sci* 2020;**21**:6454.
20. Mao R, Zong NN, Hu YJ, Chen Y, Xu Y. Neuronal death mechanisms and therapeutic strategy in ischemic stroke. *Neurosci Bull* 2022;**38**:1229−47.
21. Han L, Jiang C. Evolution of blood−brain barrier in brain diseases and related systemic nanoscale brain-targeting drug delivery strategies. *Acta Pharm Sin B* 2021;**11**:2306−25.
22. Qin C, Yang S, Chu YH, Zhang H, Pang XW, Chen L, et al. Signaling pathways involved in ischemic stroke: molecular mechanisms and therapeutic interventions. *Signal Transduct Target Ther* 2022;**7**:215.
23. Yang CJ, Hawkins KE, Doré S, Candelario-Jalil E. Neuroinflammatory mechanisms of blood−brain barrier damage in ischemic stroke. *Am J Physiol Cell Physiol* 2019;**316**:C135−53.
24. Leyton-Jaimes MF, Kahn J, Israelson A. Macrophage migration inhibitory factor: a multifaceted cytokine implicated in multiple neurological diseases. *Exp Neurol* 2018;**301**:83−91.
25. Hu JX, Ma WJ, He LY, Zhang CH, Zhang C, Wang Y, et al. Macrophage migration inhibitory factor (MIF) acetylation protects neurons from ischemic injury. *Cell Death Dis* 2022;**13**:466.
26. Chen XL, Zhang JL, Song Y, Yang P, Yang Y, Huang Z, et al. Deficiency of anti-inflammatory cytokine IL-4 leads to neural hyperexcitability and aggravates cerebral ischemia-reperfusion injury. *Acta Pharm Sin B* 2020;**10**:1634−45.
27. Guo W, Xu MM, Song XD, Cheng YJ, Deng YL, Liu M. Association of serum macrophage migration inhibitory factor with 3-month poor outcome and malignant cerebral edema in patients with large hemispheric infarction. *Neurocrit Care* 2024;**41**:558−67.
28. Liu YY, Liu YN, Wang QF, Song YD, Chen SY, Cheng B, et al. MIF inhibitor ISO-1 alleviates severe acute pancreatitis-associated acute kidney injury by suppressing the NLRP3 inflammasome signaling pathway. *Int Immunopharmacol* 2021;**96**:107555.
29. Kim J, Francis DM, Sestito LF, Archer PA, Manspeaker MP, O'Melia MJ, et al. Thermosensitive hydrogel releasing nitric oxide donor and anti-CTLA-4 micelles for anti-tumor immunotherapy. *Nat Commun* 2022;**13**:1479.
30. Ghimire K, Altmann HM, Straub AC, Isenberg JS. Nitric oxide: what's new to NO?. *Am J Physiol Cell Physiol* 2017;**312**:C254−62.
31. Angelis D, Savani R, Chalak L. Nitric oxide and the brain. Part 1: mechanisms of regulation, transport and effects on the developing brain. *Pediatr Res* 2021;**89**:738−45.
32. Sienel RI, Mamrak U, Biller J, Roth S, Zellner A, Parakaw T, et al. Inhaled nitric oxide suppresses neuroinflammation in experimental ischemic stroke. *J Neuroinflammation* 2023;**20**:301.
33. Cyr AR, Huckaby LV, Shiva SS, Zuckerbraun BS. Nitric oxide and endothelial dysfunction. *Crit Care Clin* 2020;**36**:307−21.
34. Penoy N, Grignard B, Evrard B, Piel G. A supercritical fluid technology for liposome production and comparison with the film hydration method. *Int J Pharm* 2021;**592**:120093.
35. Sun QH, Zhou ZX, Qiu NS, Shen YQ. Rational design of cancer nanomedicine: nanoproperty integration and synchronization. *Adv Mater* 2017;**29**:1606628.
36. Weltman A, Yoo J, Meng E. Flexible, penetrating brain probes enabled by advances in polymer microfabrication. *Micromachines (Basel)* 2016;**7**:180.
37. Zhang W, Liu Y, Wang Z, He S, Liu W, Wu Y, et al. Remodeling brain pathological microenvironment to lessen cerebral ischemia injury by multifunctional injectable hydrogels. *J Control Release* 2024;**369**:591−603.
38. Bi M, Gladbach A, van Eersel J, Ittner A, Przybyla M, van Hummel A, et al. Tau exacerbates excitotoxic brain damage in an animal model of stroke. *Nat Commun* 2017;**8**:473.
39. Li Y, Zou CY, Chen C, Li SX, Zhu ZY, Fan QY, et al. Myeloid-derived MIF drives RIPK1-mediated cerebromicrovascular endothelial cell death to exacerbate ischemic brain injury. *Proc Natl Acad Sci U S A* 2023;**120**:e2219091120.
40. Lambertsen KL, Finsen B, Clausen BH. Post-stroke inflammation-target or tool for therapy?. *Acta Neuropathol* 2019;**137**:693−714.
41. Choi BR, Johnson KR, Maric D, McGavern DB. Monocyte-derived IL-6 programs microglia to rebuild damaged brain vasculature. *Nat Immunol* 2023;**24**:1110−23.
42. Imai H, Masayasu H, Dewar D, Graham DI, Macrae IM. Ebselen protects both gray and white matter in a rodent model of focal cerebral ischemia. *Stroke* 2001;**32**:2149−54.
43. Tian YS, Zhong D, Liu QQ, Zhao XL, Sun HX, Jin J, et al. Upregulation of miR-216a exerts neuroprotective effects against ischemic injury through negatively regulating JAK2/STAT3-involved apoptosis and inflammatory pathways. *J Neurosurg* 2019;**130**:977−88.
44. Li L, Jiang WF, Yu BJ, Liang HQ, Mao SH, Hu XW, et al. Quercetin improves cerebral ischemia/reperfusion injury by promoting microglia/macrophages M2 polarization *via* regulating PI3K/Akt/NF-κB signaling pathway. *Biomed Pharmacother* 2023;**168**:115653.
45. Pan J, Jin JL, Ge HM, Yin KL, Chen X, Han LJ, et al. Malibatol A regulates microglia M1/M2 polarization in experimental stroke in a PPARγ-dependent manner. *J Neuroinflammation* 2015;**12**:51.
46. Bai SS, Lu X, Pan Q, Wang B, Pong UK, Yang YK, et al. Cranial bone transport promotes angiogenesis, neurogenesis, and modulates meningeal lymphatic function in middle cerebral artery occlusion rats. *Stroke* 2022;**53**:1373−85.
47. Dumbrava D, Surugiu R, Börger V, Ruscu M, Tertel T, Giebel B, et al. Mesenchymal stromal cell-derived small extracellular vesicles promote neurological recovery and brain remodeling after distal middle cerebral artery occlusion in aged rats. *Geroscience* 2022;**44**:293−310.
48. Nirwane A, Yao Y. SMA$^{low/undetectable}$ pericytes differentiate into microglia- and macrophage-like cells in ischemic brain. *Cell Mol Life Sci* 2022;**79**:264.
49. Zheng JJ, Dai QX, Han KY, Hong WD, Jia DY, Mo YC, et al. JNK-IN-8, a c-Jun N-terminal kinase inhibitor, improves functional recovery through suppressing neuroinflammation in ischemic stroke. *J Cell Physiol* 2020;**235**:2792−9.
50. Barca C, Wiesmann M, Calahorra J, Wachsmuth L, Döring C, Foray C, et al. Impact of hydroxytyrosol on stroke: tracking therapy response on neuroinflammation and cerebrovascular parameters using PET-MR imaging and on functional outcomes. *Theranostics* 2021;**11**:4030−49.
51. Liu R, Berry R, Wang L, Chaudhari K, Winters A, Sun Y, et al. Experimental ischemic stroke induces secondary bihemispheric white matter degeneration and long-term cognitive impairment. *Transl Stroke Res* 2024. Available online: https://doi.org/10.1007/s12975-024-01241-0.